3. Experimental part

3.1. Film fabrication

The details about the fabrication of the mesoporous silica films in a dip-coating process will be described in the following section. Also details about the fabrication of other films used as overlayers, PMMA and PZT, will be given. The list of the fabricated samples used in this thesis can be found in the Appendix. The code BTR-BA denotes samples synthesized by H. Bretinger and KOD-KA by D. Konjhodzic.

3.1.1. Mesoporous silica films

The coating solution for the fabrication of the mesoporous thin films was prepared according to procedures optimized in the Marlow group. The procedure consists of two steps. First, 3.435 mmol of the nonionic triblock copolymer poly(ethylene oxide)–*block*–poly(propylene oxide)–*block*–poly(ethylene oxide) ($EO_{20}PO_{70}EO_{20}$, Pluronic P123, BASF) was dissolved in 1.029 mol ethanol (C_2H_5OH) with addition of the dye Rhodamine Rh6G (0.166 mmol). Also, 0.522 mol water was added and the solution was stirred at room temperature for 10 min in the covered beaker. Two-molal hydrochloric acid HCl (2.796 mmol) was added as a catalyst and the solution was stirred until the Pluronic was totally dissolved. This Pluronic solution can be stored at 20°C for a long time.

The coating solution was prepared by mixing the silica precursor tetrabutoxysilane (TBOS, >97%, Fluka) with the Pluronic solution in a 50 ml beaker.

Exactly 10.13 g of the Pluronic solution were mixed with 23.96 mmol of TBOS (7.679 g). The mixture was stirred at room temperature for 30 minutes in the covered beaker. Resulting molar composition of the coating solution was: TBOS : P123 : H_2O : HCl : C_2H_5OH : Rh6G = 1 : 0.018 : 2.83 : 0.015 : 5.58 : 0.0009. Then a pre-reaction of this solution has been carried out for 2.5 h at 70°C. After cooling down to room temperature for 30 minutes, the weight losses, which have to be between 1 g and 2 g, were checked. The viscosity of the fresh coating solution was e.g. μ = 0.013 Ns/m^2 [96].

The used supports were 1 mm and 0.16 mm thick BK7 glass slides, freshly cleaved mica slides, (100)-silicon wafers with a thickness of 380 µm coated with a 1 µm thick amorphous silica layer, and epoxy resin blocks made of 10 g VCD, 4 g D.E.R. 736, 26 g NSA, and 0.4 g DMAE (Polysciences). The glass and Si substrates were cleaned carefully using 4 vol.% Küvettol® (Neolab) and ethanol (absolute, Merck). The films were deposited onto substrates using a dip-coater (T_O_P Oberflächentechnik GmbH) in a closed box. The box with the volume of 120 L was flushed with dried air at 350 L/h, allowing a control of humidity in the range of 32%-60%. A dipping velocity down was kept constant at 9 mm/s. After a pause of 10 s the deposition was performed with a withdrawal velocity in the range of 0.3-2 mm/s.

The samples were dried in vertical position in the desiccator at room temperature (RT) for one day. The films deposited onto all other substrates except epoxy resin were calcined by the following calcination program:

- temperature increase in 20 minutes to 100°C,
- stay at 100°C for 1 hour,
- increase the temperature to 400°C during 5.3 hours, and
- stay at 400°C for 4 hours.

After cooling the furnace itself the samples were taken out and stored in the desiccator at RT and low relative humidity (RH = 20-30%).

3.1.2. MSFs with thickness gradients

In the normal dip-coating the substrate is withdrawn vertically from the coating bath. By this way the thickness is homogeneous over the whole film. In order to determine the interplay between film thickness and processing parameters, coating

with a tilting movement was performed as shown in Figure 3.1. The microscope glass slide was dipped into the solution with the long side and withdrawn with a constant velocity at the left side. With this tilting movement one can obtain a thickness gradient over the whole sample with the biggest thickness at the left side, where the velocity is highest. Closer to the pivot (point P) the velocity is lower causing smaller thickness of the film. The velocity v_i at the point P_i of the slide can be calculated considering the geometry of the setup after:

$$v_i = v_L \frac{\sqrt{(\ell - \ell_i)^2 + h_i^2}}{\ell} \tag{3.1}$$

where ℓ is the distance between points L and P (here fixed to ℓ = 97.5 mm), ℓ_i the horizontal distance from the lifting point L, and h_i the vertical distance from $\overline{LP}$. For every point P_i with the velocity v_i, a different film thickness d_i is assigned. By this way a broad range of thicknesses can be obtained at the same processing parameters, especially at the same relative humidity.

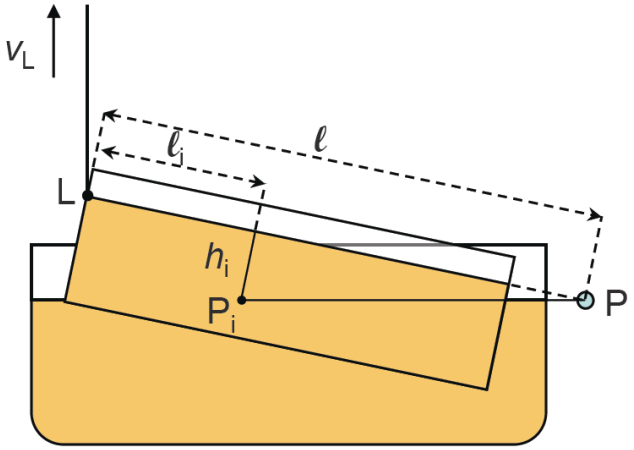

Figure 3.1: *Scheme of the setup for the coating with a tilting movement.*

3.1.3. PMMA films

PMMA films were deposited from the solution either onto BK7 glass slides or mesoporous silica films (MSFs). Poly(methylmethacrylat) (PMMA) granulates (Polysciences) with MW: 100.000 were dissolved in tetrahydrofuran (THF) by sirring at RT for one day. Either a 10 wt.% or a 15 wt.% solution was prepared. Since THF is irritant and harmful, the preparation of the solution was performed in the hood. Clean substrates were coated with the solution using either a commercial dip-coater

(T_O_P Oberflächentechnik GmbH) or a home-built “inverse dip-coater”. In the case of the inverse dip-coater the substrate was placed in the container with the solution and the solution was left to drain with a defined velocity. After drying in air for several minutes, the samples were annealed at 90°C for one day.

3.1.4. PZT films

The preparation of the coating solutions for the lead zirconate titanate (PZT) films is based on the recipe of Kozuka’s group [87]. They were prepared from starting solutions of molar compositions of $Pb(NO_3)_2$: $Zr(n\text{-}OC_3H_7)_4$: $Ti(i\text{-}OC_3H_7)_4$: PVP : $CH_3COCH_2COCH_3$: H_2O : $CH_3OC_2H_4OH$: n-C_3H_7OH = 1.1 : 0.53 : 0.47 : 1 : 0.5 : 2 : 30 : 1.24. First, lead(II)-nitrate ($Pb(NO_3)_2$, MW: 331.2 g/mol) was dissolved in 2-methoxyethanol ($CH_3OC_2H_4OH$, MW: 76.096 g/mol) by stirring at room temperature. Polyvinilpyrrolidone MW 630000 (PVP, monomer MW: 111.14 g/mol) was slowly added as a stress-relaxing agent and then acetylacetone ($CH_3COCH_2COCH_3$, MW: 100.118 g/mol) as a chelating agent. A 70 wt.% zirconium(IV)-n-propoxide solution in n-propanol ($Zr(n\text{-}OC_3H_7)_4$-n-C_3H_7OH, MW: 327.575 / 0.7 = 467.964 g/mol) and titanium(IV)-isopropoxide (i-$Ti(OC_3H_7)_4$, MW: 284.255 g/mol) were added under air exclusion. The resultant solution was refluxed at 70°C for 2 h by stirring, followed by cooling down to room temperature. The prescribed amount of ion-exchanged water was added to the solution by stirring, and the solution was kept in a sealed glass container at RT for at least 40 h before deposition.

The substrates (glass slides, Si-wafers, quartz, ITO) were cleaned with the same procedure as for the deposition of mesoporous silica films and were coated with the PZT solution using a dip-coater (T_O_P). The drawing rate was varied in the range between 0.1 and 2 mm/s. The deposited films were dried in air for one day. The temperature in the chamber was 21-23°C and the humidity varied in the range 37-50% RH depending on the day of deposition. The samples were annealed in an electric furnace in following steps:

- 10 min drying at 80°C,
- 10 min pyrolysis of organics at 300°C,
- 10 min crystallization at 600-700°C, with different heating rates.

3.2. Interferometry

The films were characterized using two different interferometric setups, one with the fixed perpendicular incidence and one with variable incidence angle, in order to measure the most important properties: film thickness *d* and refractive index *n*. These setups will be described in this Chapter.

3.2.1. Normal white light interferometry

The film thicknesses were measured using a NanoCalc 2000 white light spectrometer (Mikropack GmbH). The incidence of the white light is perpendicular to the film surface. The measurement principle exploits the interference of light in thin layers (Fabry-Pérot oscillations). Light is reflected at different interfaces, resulting in phase shifts and superposition of amplitudes and finally adding up to different intensities for different wavelengths. The scheme of the measurement principle is shown in Figure 3.2. The reflected intensity is measured as a function of wavelength and fitted with a simulated curve for a certain thickness. The measurement is quick and allows a lateral scanning of thickness profiles but it uses the refractive index of the film which has to be determined separately. The measurement of the refractive index will be discussed in Chapter 4.3. A value of *n* = 1.17 was used in all following measurements.

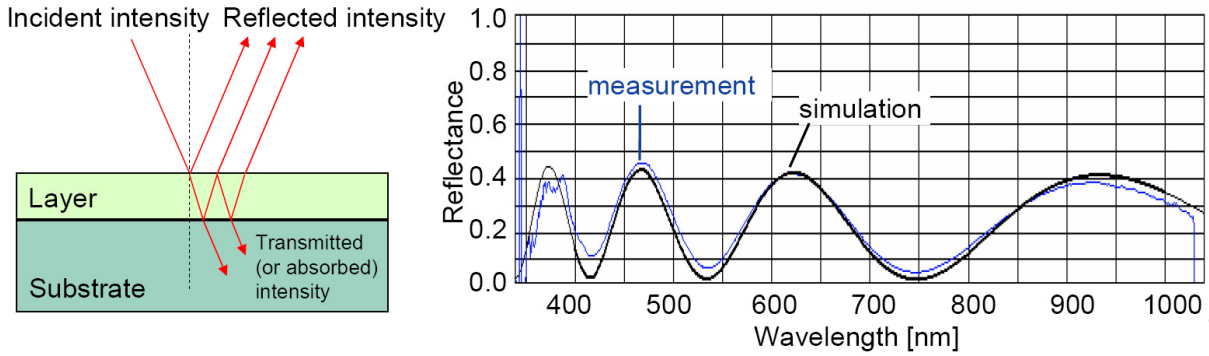

Figure 3.2: *Left: Interference of light in thin layers as a measurement principle. Right: An example (sample KOD-KA-055-07) for the determination of the film thickness (here d = 798 nm). The blue curve shows the measured reflectance and the black curve is a simulated curve for a certain thickness with defined refractive index, which best fits to the experimental curve.*

NanoCalc is doing reflectance simulations with a maximum of three layers on the bulk material. However, only the thickness of one layer can be varied. The others have to be measured separately and set fixed.

At each interface a certain amount of light is regarded as lost. This percentage has to be input as a “roughness factor”. This parameter does not change positions of the peaks, only the measured amplitude.

The reflectance of the support (BK7 glass or Si-wafer) as a reference was measured first and then the reflectance of the thin film. A typical result of the measurement looks like the right graph in Figure 3.2. The measured signal (blue curve) is fitted with the theoretical curve (black) delivering the value of the film thickness.

The film thickness of the samples prepared by the normal dip-coating was measured at five different places. Using the motor driven x-y-stage (Mapping 6’’) with the NanoCalc 2000 interferometer the whole surface of the samples coated with a tilting movement was mapped in the 3D-mapping mode. The distance between measuring points was 1 mm in both directions.

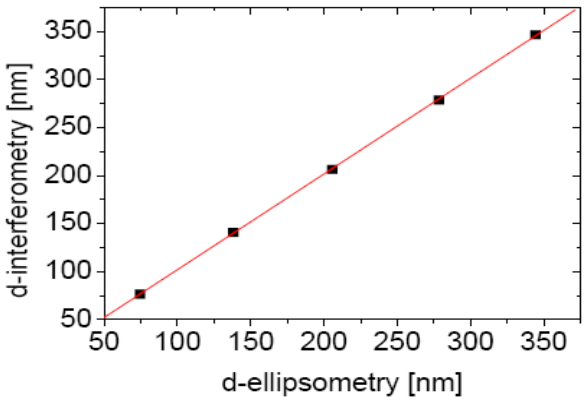

Figure 3.3: *Comparison of the thicknesses measured using white light interferometry with the ellipsometry data sheet (step wafer SiO_2 on Si, Mikropack).*

This method is very accurate for the measurement of film thickness. The error of the measurement is smaller than 2 nm estimated from the comparison with the ellipsometry data sheet for a silicon step wafer (Figure 3.3). However, this step wafer has extremely flat terraces with negligible scattering, so the measurements of the MSFs can be afflicted with bigger errors.

3.2.2. Angle-dependent white light interferometry

The refractive index was determined from the Fabry-Pérot oscillations observed in the transmission spectra, which were measured with a two-axes goniometer at different incidence angles of the light (0°, 15°, 30°, 45° and 60°). The typical measured sample area was 1 mm^2. The dependence of the transmitted intensity on the incident angle enables simultaneous determination of the film thickness and refractive index.

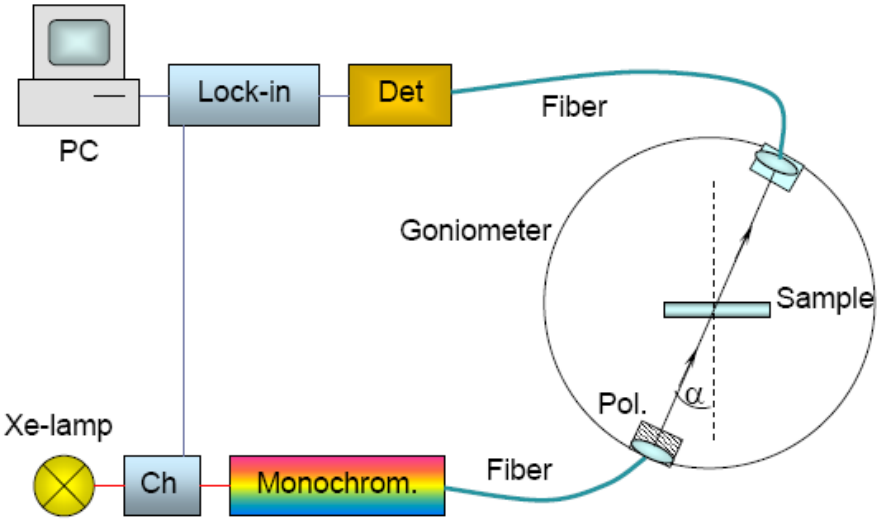

Figure 3.4: *Experimental setup for angle-dependent interferometry for the simultaneous measurement of film thickness and refractive index.*

Figure 3.4 shows the experimental setup of the angle-dependent spectrometer (Amko GmbH) [97]. The white light from a 75 W Xenon arc lamp passes a mechanical chopper and a monochromator. It is further guided via an optical fiber to the source arm of the goniometer. The light is focused with an off-axis parabolic mirror to the 1 mm spot in the centre of the goniometer. A polarizer in the source arm was used to control the light polarization, which is important for the measurements of the birefringence. After passing the film deposited on a glass slide the transmitted light enters an aperture in the detector arm and is focused with a parabolic mirror to the core of an optical fiber. The fiber is connected to a Si detector, where the signal is amplified with a lock-in amplifier. The use of optical fibers enables a free movement of both arms of the goniometer. Details about the determination of the refractive index will be discussed in Chapter 4.3.

3.3. Atomic force microscopy (AFM)

The atomic force microscope (AFM), invented in 1986 [98], exploits the local interaction between a very small tip and a sample. It is a further development of the scanning tunneling microscope [99], which can be used only for conductive samples. AFM can be driven in three basic modes:

- Contact mode, where a sharp tip on the cantilever is in permanent contact with the sample surface and its deflection is used as a feedback signal.
- Tapping mode, where the amplitude of the oscillating cantilever is measured as it is repelled or attracted to the surface due to the van der Waals forces.
- Non-contact mode, where the tip oscillates above the surface.

AFM investigations of lower resolution were performed with a Thermo Microscopes system Explorer^{TM} in Max-Planck-Institute Mülheim using tapping mode. For more detailed investigations, especially for phase images, Digital Instruments systems Dimension 3100 with Nanoscope III controller in University Ulm and Max-Planck-Institute Düsseldorf were used. The images were obtained in tapping mode with a silicon tip on the cantilever oscillating at ω = 250 kHz. This frequency was chosen slightly below the resonant frequency (automatic adjustment). The spring constant of the cantilever was 42 N/m. The devices were placed on tables with vibration damping to reduce environmental disturbances.

3.3.1. Principle of tapping mode AFM

In intermittent-contact mode or tapping mode^{TM} (Digital Instruments) the cantilever is excited with a piezo crystal at a fixed frequency, near or at its resonance frequency. The tip on the cantilever makes contact with the sample surface only for short duration in each oscillation cycle. Large amplitudes, up to 100 nm, provide the cantilever with enough energy to overcome adhesion forces. As a result of changing distances between the tip and the sample, the vibration amplitude of the cantilever is reduced compared to that of the freely oscillating cantilever. This amplitude reduction is used as a feedback parameter. In the simplified AFM model in Figure 3.5 a laser beam is reflected off a cantilever onto a mirror and then reflected onto a photodiode array as a position sensitive detector (PSD). The signal

from the PSD is rectified and lowpass filtered into a DC voltage (RMS amplitude). The feedback loop compares the RMS amplitude to the setpoint voltage and moves vibrating cantilever up or down until the RMS reaches the setpoint. This method results in lower lateral forces compared to the contact mode in which the probe slides across the surface. Therefore, the irreversible destruction on soft surfaces can be reduced.

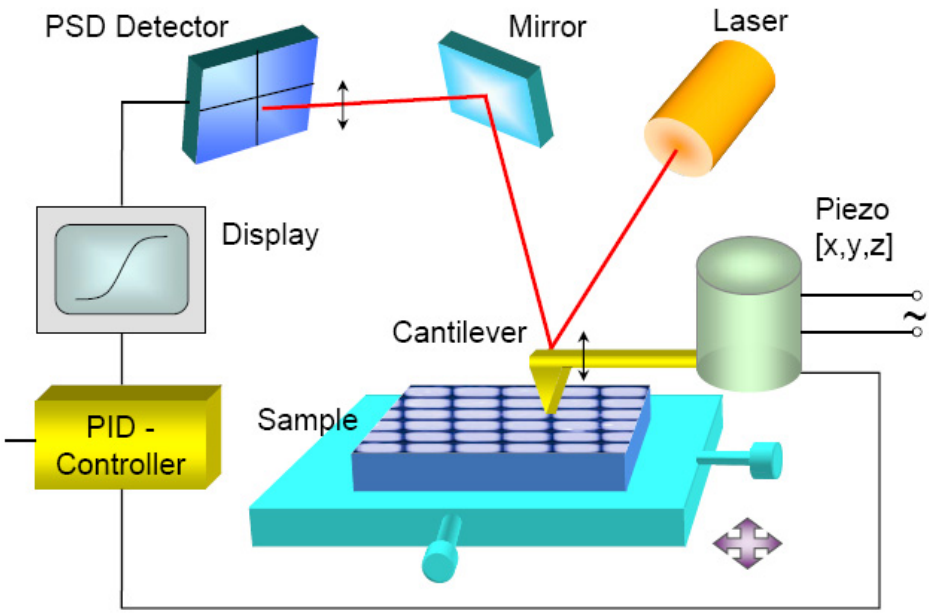

Figure 3.5: *Simplified setup of an atomic force microscope (AFM).*

Many theoretical papers have considered the dynamics of an oscillating cantilever in AFM tapping mode [100, 101]. The model most commonly used proposes an equation of motion for the tip cantilever assembly based on the model of a damped harmonic oscillator:

$$m\frac{d^2z}{dt^2} = -k_c z - \frac{m\omega_0}{Q}\frac{dz}{dt} + F_0\cos\omega t + F_{ts}(z,t) \qquad (3.2)$$

where k_c is the elastic constant of the cantilever, m is its effective mass, $\omega_0 = \sqrt{k_c/m}$ is the natural frequency of the cantilever, Q is its quality factor, z is the tip-sample distance, F_{ts} is the tip-sample interaction force and $F_0 \cdot \cos(\omega t)$ is the oscillating driving force. The damping factor γ_0 is here represented by: $\gamma_0 = m\omega_0/Q$.

The solution of harmonic oscillator with damping in absence of tip-surface forces ($F_{ts}(z, t) = 0$) has a transient term and a steady solution, which is a harmonic

function with a phase lag with respect to the excitation force and can be found for example in the textbook Demtröder [102]. For

$$z = A\cos(\omega t + \varphi) \tag{3.3}$$

the amplitude can be calculated by the Lorentz-like expression

$$A(\omega) = \frac{F_0/m}{\sqrt{\left(\omega_0^2 - \omega^2\right)^2 + \left(\omega\omega_0/Q\right)^2}} \tag{3.4}$$

and the phase angle φ by

$$\varphi(\omega) = \arctan\left(\frac{\omega\omega_0}{Q\left(\omega_0{}^2 - \omega^2\right)}\right). \tag{3.5}$$

3.3.2. Phase imaging

In phase imaging, the phase lag of the tip relative to the excitation signal is monitored and recorded. The phase angle φ in equation (3.5) varies sharply around resonant frequency and is $\varphi = \pi/2$ at $\omega = \omega_0$, smaller than $\pi/2$ for $\omega < \omega_0$, and larger than $\pi/2$ for $\omega > \omega_0$.

In the convention of the Digital Instruments Nanoscope controller, the phase shift is presented as $\Delta\varphi = \pi/2 - \varphi$ instead of the "physical phase" φ [103, 104, 105]. Therefore a zero phase shift $\Delta\varphi = 0$ corresponds to the free cantilever oscillating at resonance ($\varphi = \pi/2$), negative shifts, $\Delta\varphi < 0$, correspond to phase values φ higher than $\pi/2$ and positive ones to phase values lower than $\pi/2$.

In the case of tip-sample interaction in tapping mode, the phase angle is modified by the acting force. Magonov et al. [106] argued that the effect of tip-sample interactions could be accounted by introducing an effective force constant $k_{eff} = k_c + \sigma$, where $\sigma = \sum \partial F_i/\partial z$ is the derivative of the forces acting on the tip. The phase angle φ (in radians) of the interacting cantilever can be expressed as:

$$\varphi = \arctan\left(\frac{m\omega\omega_0}{Q\left(k + \sigma - m\omega^2\right)}\right) \tag{3.6}$$

The phase angle φ_0 (i.e. φ at ω_0) is given by:

$$\varphi_0 = \arctan\left(\frac{k}{Q\sigma}\right) \tag{3.7}$$

When σ is very small in magnitude compared with k, the phase angle shift $\Delta\varphi$ between the free and interacting cantilever is:

$$\Delta\varphi_0 = \Delta\varphi(\omega_0) = \frac{\pi}{2} - \arctan\left(\frac{k}{Q\sigma}\right) \approx \frac{Q\sigma}{k} \tag{3.8}$$

In terms of the effective interactions, and according to the convention, a negative phase shift can be correlated to an overall attractive tip-sample interaction (or more properly, a positive force gradient) and a positive phase shift to an overall repulsive one (or more properly, a negative force gradient). When the overall force derivative σ is dominated by the surface stiffness, a stiffer region has a more positive phase shift and appears brighter in a phase image.

In general, a softer material leads to a larger contact area, and the duration of tip-sample contact is longer on a soft than on a hard material [106]. These effects are enhanced at large driving amplitude A_0 and small ratio r_{sp} of the set-point amplitude A_{sp} to A_0, $r_{sp} = A_{sp} / A_0$. Consequently, a change in the stiffness can be dominated by a change in the contact area, which makes the phase shift greater on a softer than on a harder material [106].

3.3.3. Energy dissipation

In the model of Cleveland and Anczykowski [107, 108] the phase images are closely related to maps of energy dissipation. Tamayo and Garcia [109, 110] deduced an expression that relates the phase shift angle $\Delta\varphi$ to the energy E_{dis} dissipated by the tip-sample interactions per oscillation period:

$$\sin\Delta\varphi = \frac{\omega}{\omega_0}\frac{A_{sp}(\omega)}{A_0} + \frac{QE_{dis}}{\pi k A_0 A_{sp}(\omega)} \tag{3.9}$$

They have verified this model in numerical simulations and experimentally. E_{dis} was determined from the area enclosed in the loading-unloading force hysteresis. The values of the energy obtained from force curves were very similar to those deduced from this model based on phase shift measurements. It confirmed that phase images can be interpreted as maps of energy dissipation.

James et al. found out [103] that moving from the noncontact to intermittent-contact regime resulted in a contrast inversion. The most dissipative features were light in the noncontact and dark in intermittent-contact regimes.

3.4. Other experimental methods

The structure determination of the mesoporous silica films is based on small angle X-ray scattering (SAXS) and transmission electron microscopy (TEM) which will be presented in this Chapter. Scanning electron microscopy (SEM) as a method used for the characterization of structured PZT will be described afterwards as well as the UV-Vis diffuse reflectance spectroscopy for the characterization of the scattering of MSFs.

3.4.1. Small angle X-ray scattering (SAXS)

The most common tool used to identify the structure of solids is X-ray diffraction (XRD). Although the self-assembled mesostructures are not crystalline, the diffraction occurs due to the periodic contrast in electron density between the amorphous framework and pores (or surfactant regions). For the small angles presently considered, the relevant section of the Ewald sphere surface may be approximated by a plane, and 2D X-ray patterns are images of sections of the reciprocal space.

X-ray diffraction measurements were performed at grazing incidence using a General Area Detector Diffraction System (GADDS) from Bruker AXS (Figure 3.6). It utilizes a Bruker HI-STAR multiwire (1024x1024) area detector and a $CuK_{\alpha 1}$ (λ = 1.542 Å) X-ray source operated at 40 kV and 30 mA. The beam is highly collimated by crossed Göbel mirrors and a collimator with two 0.1 mm pinholes. The sample-to-detector distance was 29.9 cm. The incident angle between the beam and the film plane can be varied by rotation of the sample stage in an angle ω. The measurements were performed at an angle ω between 0.1° and 1.4°, with the collection time between 10 minutes and up to 10 hours. The obtained 2D diffractograms were unwarped (spatial correction) and saved as Tiff-images.

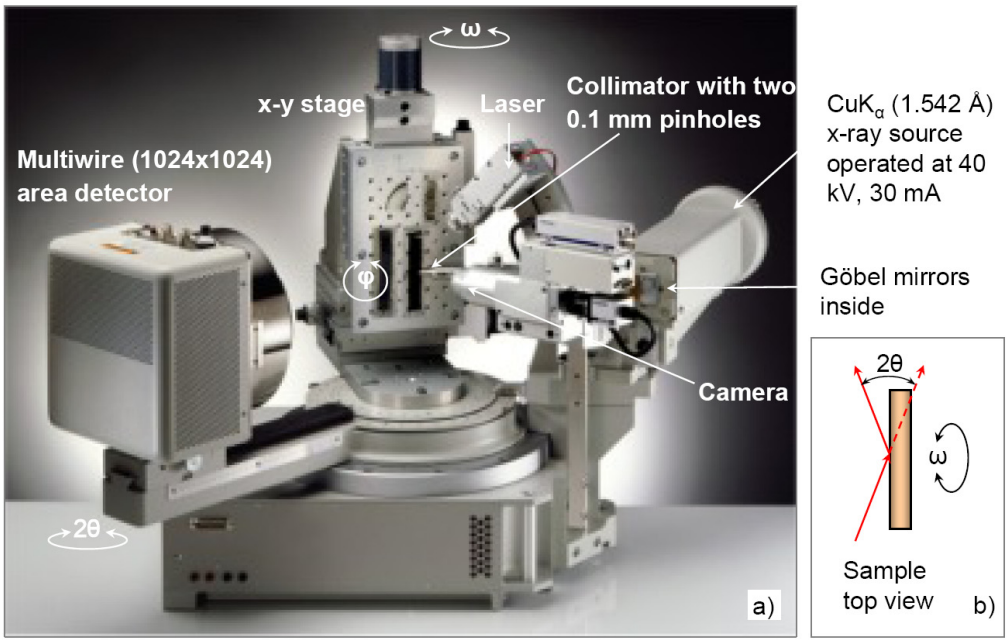

Figure 3.6: *a) General Area Detector Diffraction System (GADDS) setup used for the Small Angle X-ray Scattering (SAXS) measurements at grazing incidence. b) Top view of the sample with the primary and diffracted beams.*

3.4.2. Transmission electron microscopy (TEM)

Transmission electron microscope consists of three systems: an illumination system, an imaging system, and an image translating system [111]. The illumination system contains two units: the electron gun which is the source of electrons, and the condenser which regulates the intensity of the beam and directs it onto the specimen. The imaging system consists of an objective lens and one or more projector lenses. The image is formed at once and the information is contained in the form of variations of electron intensity over its area due to scattering and diffraction on the sample. This electron image must be converted into a visible light image by means of a fluorescent screen, photography, or a CCD camera. Other electron microscope components are the specimen chamber and holder, an objective aperture, and a vacuum system. The resolution of the microscope is limited by the wavelength of the electron beam:

$$\lambda = \frac{h}{\sqrt{2 \cdot m \cdot e \cdot U}} = \frac{12.3 \cdot 10^{-10}\,\mathrm{m}}{\sqrt{U/\mathrm{V}}} \tag{3.10}$$

where U is the accelerating voltage [111].

A Hitachi 7500 transmission electron microscope (service department MPI) operating at 22.8 kV was used for the TEM investigations. The highest possible accelerating voltage is 120 kV, the maximum resolution is 0.36 nm, and the biggest magnification is 600000x. Two fluorescent screens with diameters of 160 mm and 33 mm are used as detector.

The films on epoxy resin substrates or on freshly cleaved mica were used for investigations, because of an easier microtoming. The films were covered by a 20 nm thick gold layer as a marker to aid identification in the TEM images. Then the films were embedded in an epoxy resin made out of four components (VCD, D.E.R. 736, NSA, and DMAE) and harden at 60°C. Using an ultramicrotome with a diamond knife, 42-70 nm thick cross-sectional slices were cut. These slices were deposited onto copper grids for the TEM observation. The images were recorded with a CCD camera with the illumination time of 200 ms.

3.4.3. Scanning electron microscopy (SEM)

Scanning electron microscopy is widely employed to observe the surface of bulk samples. A finely focused beam of electrons is scanned across the sample and scattering and ionization occur near the surface. Backscattered and secondary electrons coming from the sample can be collected with a detector. The image is formed on a cathode ray tube after first converting information from the sample surface into a train of electrical signals [111]. Due to shading and the composition dependent yield of secondary electrons, topographical and materials contrast is obtained.

For the investigations a Hitachi S-3500N scanning electron microscope (service department MPI) was operated at 10 or 20 keV. The samples were coated by a 10 nm layer of gold to suppress charging effects.

3.4.4. UV-Vis diffuse reflectance spectroscopy

The spectroscopic measurements were performed with a Cary 5G UV-Vis spectrometer (Varian GmbH). Only one of the two available beam paths was used

for the measurements of the glass slide as a reference and the samples. The data interval was 1 nm and the scan rate was 120 nm/min.

The spectrometer was equipped with a Praying Mantis^{TM} sample stage (Harrick Scientific Products, Inc.) for the measurement of the diffuse reflectance spectra. The Praying Mantis incorporates two off-axis ellipsoidal mirrors. One ellipsoid focuses the incident beam on the sample at an incidence angle of 41.5°, while the second one collects the diffusely reflected radiation from the sample. Both ellipsoidal mirrors are tilted forward so the diffusely reflected radiation is collected at an azimuthal angle of 120°. This deflects the specularly reflected component behind the collection ellipsoid. A piece of white paper was used as a reference. It has nearly the same diffuse reflectance as the commonly used $BaSO_4$ powder.